ResearchGate

See discussions, stats, and author profiles for this publication at: https://www.researchgate.net/publication/263954657

Efficient Adsorption and Combined Heterogeneous/Homogeneous Fenton Oxidation of Amaranth Using Supported Nano-FeOOH As Cathodic Catalysts

ARTICLE *in* THE JOURNAL OF PHYSICAL CHEMISTRY C · JANUARY 2012

Impact Factor: 4.77 · DOI: 10.1021/jp210167b

CITATIONS
32

READS
37

3 AUTHORS, INCLUDING:

Guoquan Zhang
Dalian University of Technology
40 PUBLICATIONS **482** CITATIONS

SEE PROFILE

Available from: Guoquan Zhang
Retrieved on: 01 February 2016

THE JOURNAL OF PHYSICAL CHEMISTRY C

Article

pubs.acs.org/JPCC

Efficient Adsorption and Combined Heterogeneous/Homogeneous Fenton Oxidation of Amaranth Using Supported Nano-FeOOH As Cathodic Catalysts

Guoquan Zhang,* Shuai Wang, and Fenglin Yang

Key Laboratory of Industrial Ecology and Environmental Engineering (China Ministry of Education), School of Environmental Science and Technology, Dalian University of Technology, Dalian 116024, China

ABSTRACT: Iron oxyhydroxide (FeOOH) as heterogeneous catalyst has been widely used in Fenton-like advanced oxidation processes due to its attractive properties such as wide-operating pH range and controllable iron leaching into solution. However, little is known about the Fe^{3+}/Fe^{2+} transformation of supported FeOOH catalyst under the external electrical field condition, which is of the essence in electro-Fenton-like oxidation reactions. In this study, activated carbon-supported nano-FeOOH (FeOOH/AC) catalysts were prepared by the air oxidation of ferrous hydroxide suspension method. The as-prepared catalyst was characterized with various characterization techniques and identified as goethite and lepidocrocite mixed crystals. Adsorption and electrochemically assisted oxidation of amaranth with the FeOOH/AC heterogeneous catalysts were investigated at pH 4.0 using graphite felt as cathode. Under weak acidic and external electric field conditions, the supported nano-FeOOH catalyst undergoes proton-promoted dissolution and electrochemical reductive dissolution processes, which facilitates Fe^{3+}/Fe^{2+} transformation and produces a beneficial enhancement of the heterogeneous/homogeneous electro-Fenton reaction rates. Experimental results demonstrated that the FeOOH/AC heterogeneous catalyst possesses admirable adsorbability, and the electrochemically assisted oxidation of amaranth takes place not only through the heterogeneous Fenton reaction on catalyst/solution interface but also through the homogeneous Fenton reaction in bulk solution due to iron liberation from the supported nano-FeOOH. In addition, a possible electrochemically assisted oxidation mechanism is also proposed.

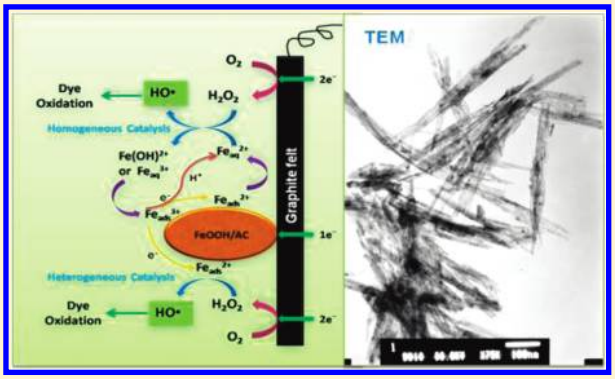

1. INTRODUCTION

In recent years, advanced oxidation processes (AOPs) that make use of various combinations of O_3, H_2O_2, UV, ultrasound, supercritical water, pulsed corona discharges, electron beam irradiation, and so on are becoming more and more important technologies for wastewater treatment, especially for high content of organics, high colority, and nonbiodegradable contaminants. These processes based on hydroxyl radical ($HO^{\bullet}$, E^{o} = 2.80 V vs SHE) chemistry have been widely applied to degrade organic pollutants due to the nonselective oxidation property of $HO^{\bullet}$. However, the homogeneous Fenton process has significant disadvantages such as narrow working pH range, iron sludge treatment, and iron ions deactivation and loss. To overcome these drawbacks, some efforts have been made to develop different heterogeneous (photo-)Fenton-like catalysts. Most of the iron sources studied include synthesized and natively found iron oxides, such as goethite,[1−4] lepidocrocite,[5,6] magnetite,[7] hematite,[8] pyrrhotite,[9] ferrihydrite,[10] Fe@Fe_2O_3 core−shell nanowire,[11] iron vanadate,[12] and different iron species supported on different inert solid supporters.[13−15] Sánchez-Sánchez et al.[1] reported that their proposed goethite-catalyzed heterogeneous electro-Fenton process yields 95% of mineralization of aniline under optimum standard electro-Fenton conditions, using only 2 ppm of soluble iron compared with 55 ppm of soluble iron used in the homogeneous process. The main advantages of these heterogeneous (photo-)Fenton-like processes are the lower concentrations of iron in the solution[1] and the easy recycling of the remaining iron catalyst. These heterogeneous catalysts were demonstrated to be efficient in the degradation of organic pollutants in wastewater over a wider applicable pH range through homogeneous reaction, dissolving iron ions into the solution, or through heterogeneous reaction, reacting at the iron oxide surface.[16,17]

It was noticed that the application of FeOOH heterogeneous catalysts was mainly concentrated on facilitating catalysts separation, employing sustained solid compounds to avoid more complex post-treatments of colloidal iron sludge. However, no attention was paid to whether the external electric field in heterogeneous Fenton-like system makes it possess the superior oxidation property by the beneficial enhancement of Fe^{3+}/Fe^{2+} transformation. In addition, the

Received: October 23, 2011
Revised: December 2, 2011
Published: January 10, 2012

 © 2012 American Chemical Society dx.doi.org/10.1021/jp210167b | *J. Phys. Chem. C* 2012, 116, 3623−3634

electrochemical advanced oxidation processes (EAOPs) based on the in situ electrogeneration of H_2O_2 from oxygen reduction reaction (ORR) have become safer and more convenient alternative for decontamination treatments[1,18−22] because they are environmentally clean and can generate large amount of $HO^{\bullet}$ under control of applied current density and/or potential.

The bove mentioned situation inspired us to (1) prepare the activated carbon-supported nano-FeOOH (FeOOH/AC) catalyst because FeOOH combined some attractive properties such as (i) wide range of operating pH, (ii) controllable leaching of iron into the solution, and (iii) excellent adsorption performance for large-scale applications[2−4] and (2) build an electrochemically assisted oxidation system, in which the regeneration of Fe^{2+} could be efficiently facilitated to activate H_2O_2 electrogenerated in situ on cathode and then produce beneficial enhancements of the heterogeneous/homogeneous Fenton reaction rates. This was referred to as the heterogeneous electrocatalytic wet peroxide oxidation (ECWPO) system in this Article. Azo dye amaranth (IUPAC name: trisodium 3-hydroxy-4-(4-sulphonato-1-naphthylazo)-naphthalene-2,7-disulphonate) was chosen as the model compound because it is environmentally hazardous and is a biological recalcitrant compound. Furthermore, even low concentration of dyes in the effluents is a source of turbidity and nonaesthetic pollution, and their discharge is particularly troublesome.[18,21] The study was mainly focused on three aspects: (i) synthesis and characterization of the FeOOH/AC heterogeneous catalysts; (ii) evaluation on the adsorption and combined heterogeneous/homogeneous oxidation performances of the FeOOH/AC heterogeneous catalysts in the ECWPO system toward amaranth degradation, and (iii) discussion of the possible oxidation mechanism of the electrochemically assisted oxidation process in this ECWPO system.

2. EXPERIMENTAL SECTION

2.1. FeOOH/AC Catalyst Fabrication. The FeOOH/AC heterogeneous catalyst was prepared by air oxidation of ferrous hydroxide suspension method. First, 200 g coal property columnar active carbon (Φ 4 mm) was added to 300 mL of 0.2 mol L^{-1} well-stirred and N_2-saturated $FeSO_4$ solutions. Then, 0.4 mol L^{-1} NaOH solution was added dropwise, and compressed air with flow rate at 2.2 L min^{-1} was insufflated concurrently into the mixture at 20 ± 1 °C. When the final pH achieved at 6.7, the oxidation reaction terminated, as revealed by the orange color of suspension. The resulting yellowish brown FeOOH/AC solid catalyst was filtrated and washed with deionized water, followed by being dried in an oven at 40−50 °C for 24 h (inset of Figure 1).

2.2. FeOOH/AC Catalyst Characterization. The AC support and the FeOOH/AC heterogeneous catalyst were characterized using the following techniques:

- The iron content of the FeOOH/AC heterogeneous catalyst was dissolved via digestion treatment and analyzed using an inductively coupled plasma emission spectroscopy (ICPS-7500, Shimadzu, Japan). The ICP result is 3.12 wt %.
- Specific areas of the FeOOH/AC heterogeneous catalysts were computed from the N_2 adsorption−desorption isotherms measured at 77.3 K by applying the Brunauer−Emmett−Teller (BET) method in Quantachrom NOVA4200e. The pore size distribution, pore volume, and average pore diameter were determined by the BJH (Barrett−Joyner−Halenda) method, and the pore diameter distribution was calculated from desorption branch of the isotherm.
- The morphology of the resulting FeOOH/AC heterogeneous catalyst was investigated by environmental scanning electron microscopy (SEM, FEI Quanta 200 FEG, The Netherlands) combined with energy-dispersive X-ray spectroscopy (EDX) for element mapping (Phillips-FEI, 30 KV).
- Powder X-ray diffraction (XRD) measurements of the supported nano-FeOOH heterogeneous catalyst were carried out on a Japan Rigaku D/max-2400 (λ = 1.54056 Å) operating at 40 kV and 200 mA. The pattern was taken over the 2θ range from 20 to 80° using a position-sensitive detector with a step size of 0.02°. Diffraction pattern was manually analyzed and identified in comparison with PCPDFWIN (2002) XRD analysis software.
- Transmission electron microscopy (TEM, Tecnai G2 Spirit) operated at 120 kV was used to study the morphology and particle size of the supported nano-FeOOH heterogeneous catalyst. The sample was supported on a copper mesh for the TEM analysis.
- The chemical structure of the FeOOH/AC heterogeneous catalyst was investigated with KBr-pellets using a Fourier transfer infrared spectrometer (FT-IR, Shimadzu 8400S).

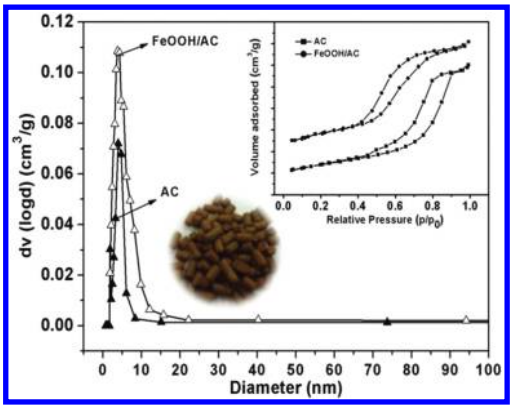

Figure 1. Pore size distribution of FeOOH/AC and AC support and N_2 adsorption−desorption isotherms of FeOOH/AC and AC support. Inset: Photograph of the as-prepared FeOOH/AC heterogeneous catalysts.

2.3. Adsorption Kinetics and Isotherms. To determine the kinetics of adsorption process, we performed adsorption experiment by adding 40−80 g (three levels) of the FeOOH/AC heterogeneous catalysts in 400 mL of 80 mg L^{-1} amaranth solution under the open circuit condition. At several points in time, the concentration of freely dissolved fraction of dye was determined spectrophotometrically (Shimazu type AA-630-01). Adsorption isotherm experiment was carried out at room temperature and pH 4.0. The 150 g L^{-1} FeOOH/AC heterogeneous catalyst was placed in a conical flask containing amaranth aqueous solutions at different initial concentrations from 10 to 80 mg L^{-1}. After adsorption for 4 h, the equilibrium concentration of amaranth in the solution was measured. The adsorbed concentrations were calculated according to eq 1

dx.doi.org/10.1021/jp210167b | J. Phys. Chem. C 2012, 116, 3623−3634

$$q_e = \frac{(c_0 - c_e)V}{M_s} \quad (1)$$

where q_e (mg g^{-1}) is the equilibrium adsorbed concentration, c_0 (mg L^{-1}) is the initial solution concentration, c_e (mg L^{-1}) is the equilibrium solution concentration, V (mL) is the volume of solution, and M_s (g) is the mass of solid sorbent.

2.4. ECWPO System Construction and Amaranth Degradation. In this study, an undivided electrochemical cell was used in the ECWPO system. To aviod the occurrence of short-circuit between anode and cathode through the accumulational FeOOH/AC heterogeneous catalyst, the anode and cathode regions were separated by a stainless-steel mesh. The volume ratio of anode compartment to cathode compartment is about 1:3. During the experiments, ca. 300 mL of catholyte and ca. 100 mL of anolyte were used. The anode was platinum sheet (10.5 cm^2), and cathode was graphite-felt (25 cm^2), which was buried beneath the accumulational FeOOH/AC heterogeneous catalyst with the loading mass in the range of 40−80 g. To electrogenerate H_2O_2 in situ effectively, we bubbled high purity oxygen into the reactor. Cyclic voltammetry measurements were carried out using an EG&G PAR 263A potentiostat/galvanostat. A saturated calomel electrode (SCE) placed in cathodic chamber was used as the reference electrode. The off-line analysis of accumulated H_2O_2 in the absence of FeOOH/AC heterogeneous catalyst was carried out with titanium salt (potassium titanyl oxalate)-spectrophotometric method (Shimadzu UV-1700) by measuring the absorbance at λ = 408 nm,[19,20] whereas in the presence of FeOOH/AC heterogeneous catalyst the accumulated concentration of H_2O_2 was measured spectrophotometrically at λ = 352 nm with the iodide reagent (0.4 mol L^{-1} KI, 60 mmol L^{-1} NaOH and 0.1 mmol L^{-1} ammonium molybdate). Electron paramagnetic resonance (EPR) spectrum was recorded at room temperature with ELEXSYS 300 spectrometer X-Band (Bruker, Germany) equipped with an in situ irradiation source (Quanta-Ray Nd:YAG laser, λ = 532 nm). 5,5-Dimethyl-1-pyrroline-*N*-oxide (DMPO, Japan) was used as the radical trapping agent. The following parameters were used for EPR experiment: microwave power 12.7 mW, microwave frequency 9.78 GHz, modulate frequency 100 kHz, and scan speed 0.3 mT min^{-1}. Soluble iron was detected by an atomic absorption spectrophotometer (Shimazu type AA-630-01) after filtering an aliquot through a 0.45 μm membrane filter. Fe^{2+} concentration was determined by the light absorption of its colored complex with 1,10-phenantroline at 508 nm.[1] Fe^{3+} concentration was calculated as the difference between the total iron and Fe^{2+} concentrations.

The electrolyte contained 80 mg L^{-1} of amaranth azo dye, and 0.2 mol L^{-1} of Na_2SO_4 was used as the supporting electrolyte. The electrolysis experiments were performed with constant potential mode controlled by a potentiostat/galvanostat electrochemical workstation (Shanghai REX Instrument Factory) at room temperature. Amaranth solution withdrawn from reactor at regular time intervals was measured spectrophotometrically. The normalized decolorization rate was followed from the drop of absorbance at the maximum wavelength λ_{max} = 521 nm calculated by eq 2.[20]

$$\text{color remove } (\%) = \frac{A_0 - A_t}{A_0} \times 100 \quad (2)$$

where A_0 and A_t are the absorbance values at λ_{max} = 521 nm for treatment time 0 and t, respectively. Dissolved organic carbon (DOC) was determined using a total orangic carbon (TOC) analyzer (Shimadzu 5050 TOC-VCPH).

2.5. Selection of Operating pH. It is well known that the operating pH of the heterogeneous Fenton-like processes was subjected to a wide range of variations and had a strong effect on the feasibility of Fenton-like process. Some authors considered that at a pH range from 4.4 to 7.0 the reaction is just heterogeneous.[5,23−26] Watts et al.[26] even suggested that a nonradicals mechanism involving electron transfer at the mineral surface or the generation of transient oxygen species was responsible for organic pollutants degradation in the neutral pH system. While at pH below 4.0, the homogeneous catalysis is of increasing importance because of the chemical reductive dissolution of iron oxides.[5,6] With a different point of view, other authors considered that at pH between 3.0 and 4.0 the solid iron species acts as a dissolved irons source in solution, and the process behaves mainly as a homogeneous Fenton reaction.[27−29] Recently, it is found that the fastest rates of the heterogeneous Fenton-like reactions in solution were observed at 3.0 ≤ pH ≤ 5.5.[30−32] Now it is very clear that at neutral pH the heterogeneous Fenton-like systems were not achieved very attractive organic pollutants degradation efficiency due to the noncontributive H_2O_2 consumption and the sedimentation of the leaching iron in solution.[2,5,6] Therefore, the need for achieving pH adjustion under mild acidic conditions for the heterogeneous Fenton-like system is one of the most important aspects to enhance the treatment effect from the viewpoint of the practical. In fact, some of the most recent studies have reported working at pH close to 5.0[30,31] to search for a plausible and practical reaction scheme. Therefore, we adopted the most typical condition of pH 4.0 in this study after the analysis of the above-mentioned literature. With regard to the influence of medium pH on ORR, it must be emphasized that no distinct difference in the H_2O_2 accumulative concentration was found in the pH range of 2.5−7.0 because the rate-determining step of H_2O_2 electrogeneration was not the interaction between the H^+ and O_2 but between the electron and O_2 ($O_2 + e^- \rightarrow O^{2-}$).[33]

3. RESULTS AND DISCUSSION

3.1. Characterization of the FeOOH/AC Catalyst. The surface area, pore diameter, and pore volume of AC support and the FeOOH/AC heterogeneous catalyst samples were characterized by N_2 adsorption/desorption. The data are listed in Table 1. The results show that the loading nano-FeOOH on

Table 1. Surface Area, Pore Diameter and Pore Volume of AC Support and the FeOOH/AC Heterogeneous Catalyst

	AC	FeOOH/AC
average pore diameter/nm[a]	3.097	3.818
total pore volume/cm^3 g^{-1}[b]	0.29	0.38
specific surface area, S_{BET}/m^2 g^{-1}[c]	602.8	412.9

[a]Average pore diameter, determined by the BJH cumulative desorption method; values were calculated by 4 V/A. [b]Single-point total pore volume of pores at P/P_0 = 0.990759. [c]BET surface area calculated from the linear part of the BET plot.

AC support decreased its specific surface area, but average pore size and total pore volume increased slightly, resulting in a higher overall porosity than AC support. This result is in

dx.doi.org/10.1021/jp210167b | J. Phys. Chem. C 2012, 116, 3623−3634

agreement with the fact that in general iron phases have low area and AC is responsible for providing high specific surface area. The N_2 adsorption/desorption isotherms of AC support and the FeOOH/AC heterogeneous catalyst samples are shown in the inset of Figure 1. Both of the profiles reveal a typical shape of Type IV curves with the Type H1 hysteresis loops, indicating the presence of mesopores structure at relative pressure range between 0.4 and 0.9.[12,34] By contrast, the N_2 adsorption/desorption isotherms of the FeOOH/AC heterogeneous catalyst exhibit a higher adsorption/desorption shape, which implies that the synthesized FeOOH/AC heterogeneous catalysts consist of compacts of approximately uniform particles with a narrow range of pore size distribution.[35,36] Figure 1 illustrates that the pore volume of the FeOOH/AC heterogeneous catalyst varied against pore size in the main range of 2−80 nm with maximum portion at ∼3.8 nm. It is obvious that the FeOOH/AC heterogeneous catalyst exhibits slightly wider pore size distribution than that of AC support, but the two samples still show the narrow pore size distributions. The results implied that the FeOOH/AC heterogeneous catalyst retained a uniform mesostructure of AC support.

SEM analysis shown in Figure 2A reveals that the AC support consists of microparticles with irregular morphology,

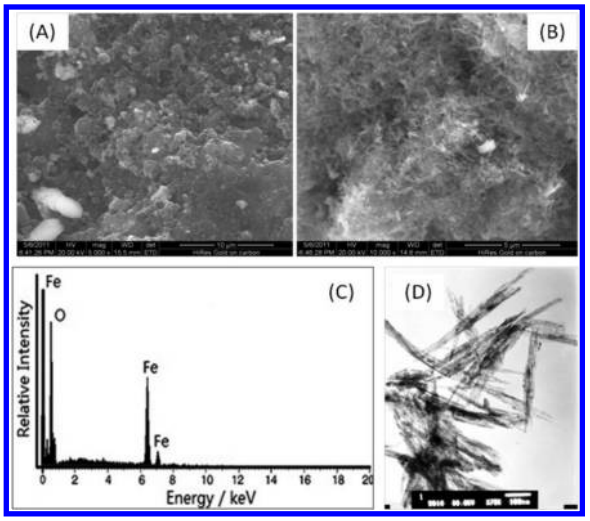

Figure 2. (A,B) SEM images of AC support and the FeOOH/AC heterogeneous catalysts, respectively, (C) EDX of FeOOH powders, and (D) TEM image of the FeOOH/AC heterogeneous catalysts.

and the particle size varies in a wide range. By contrast, the SEM morphology of the FeOOH/AC heterogeneous catalyst in Figure 2B exhibits that the heteronanostructured iron was successfully loaded on AC support. The product is of numerous honeycomb needle-like structures with ∼100% coverage rate and is uniform in size. The origin of the morphological difference between the two samples most likely lies in the loading of nano-FeOOH on AC support. Figure 2C shows the result of an EDX spectrum microanalysis of FeOOH powder recycled after synthesizing the FeOOH/AC heterogeneous catalyst and dried at 40−50 °C for 24 h, which confirms that Fe and O are the major elements, indicating that the nano-FeOOH sample is not contaminated with other elements during the preparation process. The TEM photograph of the supported nano-FeOOH/AC heterogeneous catalyst is shown in Figure 2D. The crystals are found to be either elongated or randomly aggregated rhombohedral or plate-like with the characteristic of dendritic-like or acicular structures. The sizes range from a thickness of <5 nm to a length of >100 nm. The crystallites are in contrast with the micrographs previously reported,[37,38] indicating a mixture of plate-like lepidocrocite (γ-FeOOH) particles and needle-like goethite (α-FeOOH) particles.

Figure 3A shows the XRD pattern of the as-synthesized FeOOH/AC heterogeneous catalyst. The strong and sharp

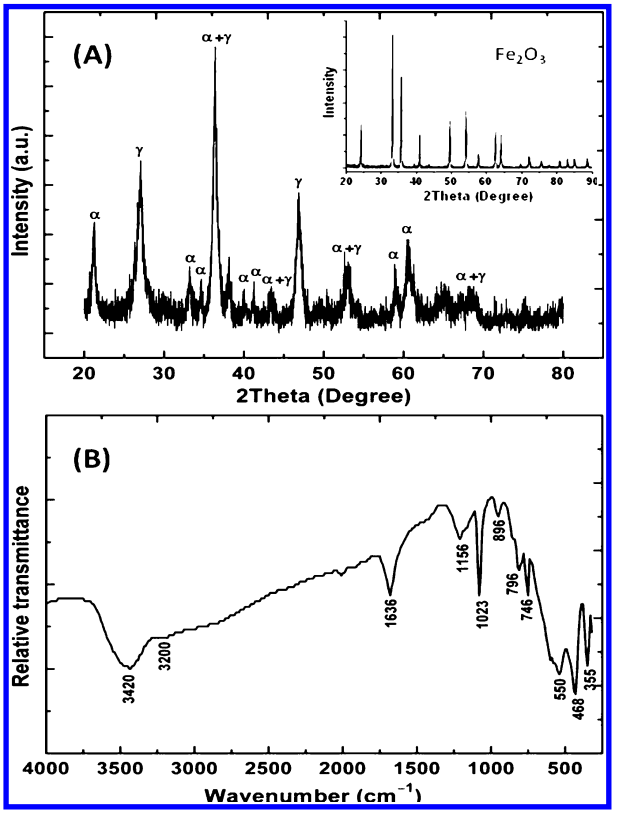

Figure 3. (A) XRD and (B) FT-IR patterns of the FeOOH/AC heterogeneous catalysts. The inset in panel A is XRD pattern of the pure Fe_2O_3 powder.

whole-angle diffraction peaks imply that all diffraction peaks can be indexed to pure orthorhombic structure. The XRD pattern with the four most intense peaks at 2θ = 27, 37.5, 47, and 53° is expected for lepidocrocite,[39,40] which are consistent with the values in the standard card (JCPDS (2002) no. 44-1415). Also present are several weaker diffraction peaks loaded at 2θ = 22, 33, 34, 37.5, 42, 58, and 62°, which were determined to be goethite indexed to the standard card (JCPDS (2002) no. 29-0713).[2,39,40] In comparison with the XRD pattern displayed in the inset of Figure 3A, it is obvious that no α-Fe_2O_3 crystalline phase constituents were formed in the supported nano-FeOOH sample. The above XRD result implies the presence of lepidocrocite with small amounts of goethite on the as-synthesized catalyst surface, and the similar results have also been reported by Cornell and Schwertmann[41] in the preparation of nano-FeOOH using the air oxidation of $Fe(OH)_2$ suspension method.

The FT-IR spectrum of the FeOOH/AC heterogeneous catalyst in Figure 3B exhibited a wide band at 3420 cm^{-1} attributed to H−O−H stretching vibration and H−O−H bending vibration located at 1636 cm^{-1}, thus indicating the

dx.doi.org/10.1021/jp210167b | J. Phys. Chem. C 2012, 116, 3623−3634

presence of adsorbed H_2O.[42] The spectrum showed a broadened IR band at 1156 cm^{-1} and two sharp bands at 1023 and 746 cm^{-1}. These IR bands can be assigned to lepidocrocite in accordance with the result of a group-theoretical analysis of the IR spectrum of lepidocrocite, as reported in the literature.[38,41−44] The IR bands at 896 and 796 cm^{-1} were the characteristic Fe−O−H bending vibrations peaks of goethite;[38,41−44] additionally, the IR band at 3200 cm^{-1} can be assigned to stretching Fe−O−H vibrations. The FT-IR result also testified the coexistence of goethite and lepidocrocite on the FeOOH/AC heterogeneous catalyst surface. Combining the results of N_2 adsorption−desorption, XRD, ICP, and FT-IR techniques, it can be deduced that the incipient wetness impregnation and the later air oxidation of ferrous hydroxide suspension is a good method to prepare supported nano-FeOOH catalysts.

3.2. In Situ Electrogeneration of H_2O_2 on Graphite-Felt Cathode. It is well known that the electrochemical advanced oxidation of organic pollutants is generally related to the amount of $HO^•$ radicals in bulk solution produced by the Fenton's reaction 4, where H_2O_2 is generated in situ by ORR on various cathode materials such as gas diffusion electrodes,[1,17−21] reticulated vitreous carbon,[45] or graphite-felt[46] following reaction 3

$$O_2 + 2H^+ + 2e^- \rightarrow H_2O_2 \quad (3)$$

$$Fe^{2+} + H_2O_2 + H^+ \rightarrow Fe^{3+} + HO^• + H_2O \quad (4)$$

As reported by many authors,[18,21,46−49] the production rate of H_2O_2 on the carbon-base cathode is affected by the applied potential or current density. To investigate the optimal reduction potential of dissolved oxygen on graphite-felt cathode, the ORR was investigated in pH 4.0 N_2- and O_2-saturated 0.2 mol L^{-1} Na_2SO_4 solutions with and without the FeOOH/AC heterogeneous catalysts. As seen from Figure 4A, an intense reduction current is observed with two-reduction peaks (−0.30 and −0.64 V) in O_2-saturated electrolyte in the absence of the FeOOH/AC catalyst, whereas in the N_2-saturated case no reduction peak is observed, which indicates that the reduction current in O_2-saturated solution must be due to catalyzed ORR. This result is in accordance with the previous reports[48,50] that ORR on carbon-based electrode proceeds in parallel at two different sites: the first is a very active surface quinone group (−0.30 V), and the second behaves as a heterogeneous electrode surface (−0.64 V) according to reaction 2. At latter potential, H_2O_2 would be fast and efficiently electrogenerated in situ. While in the presence of 150 g L^{-1} FeOOH/AC heterogeneous catalyst, an unsmooth cyclic voltammogram characterized by the reduced ORR peak current at −0.64 V was obtained. The reason for this phenomenon is probably that the mass transfer of dissolved oxygen from bulk solution to cathode/solution interface was hindered by the FeOOH/AC heterogeneous catalyst. In addition, it must be pointed out that no ferric reduction peak was observed during the cyclic voltammetric measurement, which is probably that the small ferric reduction current was covered with the large background current (charge/discharge capacitance of cathode) and oxygen reduction current.

As seen from Figure 4B, the accumulated concentration of H_2O_2 in the absence of FeOOH/AC heterogeneous catalyst reached a steady value of ca. 500 μmol L^{-1} for 180 min electrolysis at −0.64 V, and it did not increase obviously after that, suggesting a balance between anodic decomposition and

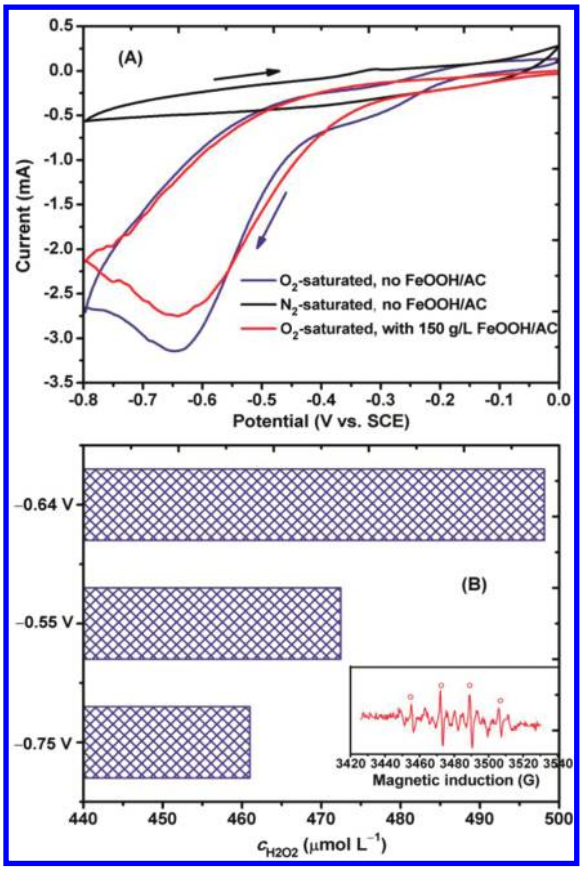

Figure 4. (A) Cyclic voltammograms of graphite felt cathode in pH 4.0 N_2- and O_2-saturated 0.2 mol L^{-1} Na_2SO_4 solutions with and without the FeOOH/AC heterogeneous catalyst. Scan rate: 20 mV s^{-1}. (B) Time course of accumulated H_2O_2 concentrations during ORR at different cathodic potentials in the absence of FeOOH/AC heterogeneous catalyst. Inset: EPR spectrum of spin adduct of DMPO-$HO^•$ produced by the FeOOH/AC heterogeneous catalyst.

cathodic production of H_2O_2 in the electrolysis system. Other two cathodic potentials (−0.55 and −0.75 V) were also applied but resulted in much lower accumulative concentration of H_2O_2 in the same electrolysis time. The reason for this phenomenon is that a more positive or negative cathodic potential resulted in a significant decrease in reduction current (Figure 4A); additionally, the side reactions such as H_2O_2 further reduction or H_2 evolution occurred at more negative cathodic potential, thus decreasing the current efficiency of H_2O_2 generation, whereas in the presence of FeOOH/AC heterogeneous catalyst, no accumulated H_2O_2 was detected by this highly sensitive iodide reagent-spectrophotometric measurement method for 180 min electrolysis at −0.64 V. We thought this phenomenon was not an indication that no H_2O_2 was electrogenerated in the electrolysis system. So, it may be inferred that the electrogenerated H_2O_2 was consumed completely through the homogeneous and heterogeneous Fenton reactions. To confirm the production of $HO^•$ by the FeOOH/AC heterogeneous catalyst, the EPR spin-trap technique was employed with DMPO as radical trapper. The above electrolyzed solution mixed with 80 mmol L^{-1} DMPO; then, the mixture solution was quickly moved into quartz tube to start the EPR measurement. As depicted in the inset of Figure 4B, the characteristic four signal peaks of DMPO-$HO^•$ adduct with peak intensity ratio of 1:2:2:1 were observed. This ligand−metal-radical complex suggested the formation of $HO^•$ in the

dx.doi.org/10.1021/jp210167b | J. Phys. Chem. C 2012, 116, 3623−3634

electrolysis system.[51] This result confirmed that HO• is truly responsible for the electro-Fenton-like oxidation treatment.

3.3. Direct and Indirect Electrochemical Oxidation in the Absence of FeOOH/AC Catalysts. To investigate the direct and indirect electrochemical oxidation performance of the electrolysis system, we electrolyzed 80 mg L^{-1} pH 4.0 amaranth solution at cathodic potential of −0.64 V in the absence of FeOOH/AC heterogeneous catalysts through three trials. Under N_2-saturated condition, the direct anodic oxidation was performed using a 10.5 cm^2 platinum as anode (trial I: AO-Pt). Under O_2-saturated condition, a cathode of 25 cm^2 graphite felt and an anode of 10.5 cm^2 graphite sheet were used to investigate the indirect cathodic oxidation (trial II: E-H_2O_2). The combined anodic and cathodic oxidation was performed also under O_2-saturated condition using graphite felt as cathode and platinum as anode (trial III: AO-Pt−E-H_2O_2). Note that the preliminary open circuit experiments showed that the color removal of amaranth is not affected in the absence of FeOOH/AC heterogeneous catalyst. Therefore, we suggested that amaranth adsorption on graphite felt cathode can be considered negligible. This may result from the microporous structure of the graphite felt, which is smaller than the size of the dye molecule.

As seen from Figure 5, the trial I results in a poor dye color removal efficiency of ca. 10% after 240 min electrolysis,

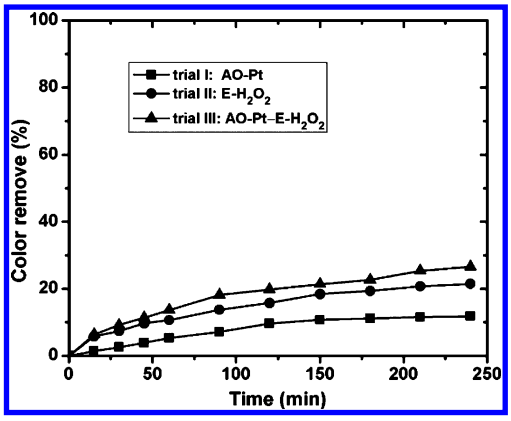

Figure 5. Amaranth color abatement rate with time during direct anodic oxidation (■), indirect cathodic oxidation (●), and the combined anodic and cathodic oxidation (▲). Initial amaranth concentration: 80 mg L^{-1}; solution pH: 4.0; cathodic potential: −0.64 V.

indicating the inefficient oxidizability of heterogeneously electrogenerated Pt(HO•) at platinum anode via eq 5. This phenomenon can be explained by the very low oxygen evolution overpotential of platinum electrode.[18,21] Another disadvantage of this electrode is that the HO• are chemisorbed and thus strongly attached to platinum surface but less reactive.

$$Pt + H_2O \rightarrow Pt(HO^{\bullet}) + H^+ + e^- \quad (5)$$

On the contrary, an obvious increase in dye color abatement can be observed in trial II, which leads to ca. 22% decolorization rate of the amaranth solution. Therefore, the contribution of H_2O_2 electrogenerated in situ at the graphite felt cathode by ORR cannot be considered to be negligible, although the oxidation power of sole H_2O_2 is finite. In the case of trial III, only a slight increase in dye color decay was obtained. The reason for this phenomenon is that the oxidation of H_2O_2 electrogenerated at cathode will take place at platinum anode through eq 6, which produces a small quantity of hydroperoxyl radical ($HO_2^{\bullet}$) possessing higher oxidation capability than H_2O_2.

$$H_2O_2 \rightarrow HO_2^{\bullet} + H^+ + e^- \quad (6)$$

The above results indicate that even a combination of anodic and cathodic oxidation of the dye is not able to reach an efficient color abatement due to the relatively small amount and less efficiency of heterogeneous Pt(HO•) and the low oxidation capacities of H_2O_2 and $HO_2^{\bullet}$ compared with the homogeneous HO• radicals.

3.4. Kinetics and Isotherms of Amaranth Adsorption on the FeOOH/AC Catalysts. To identify the individual contribution of adsorption and electrochemically assisted oxidative decolorization processes, adsorption experiments of 80 mg L^{-1} amaranth on the FeOOH/AC heterogeneous catalysts with various loadings were performed first (Figure

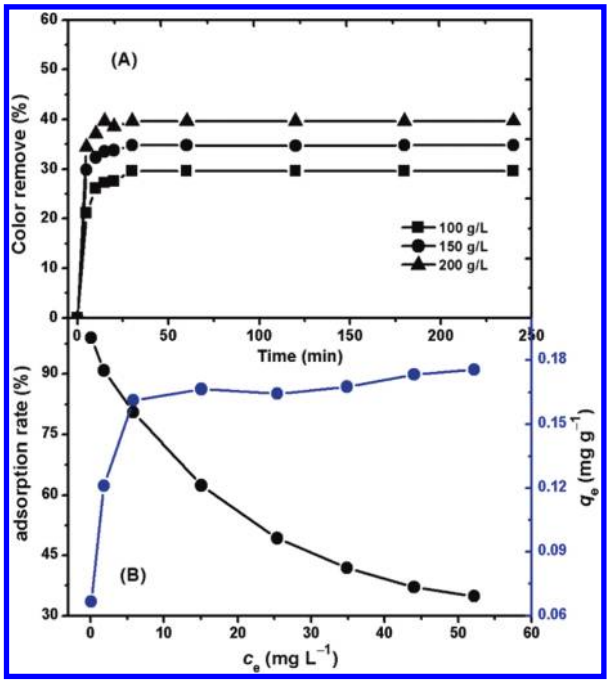

Figure 6. (A) Adsorption of amaranth on the FeOOH/AC heterogeneous catalysts with different loading amounts as a function of the contact time at room temperature (c_0: initial concentration of amaranth, 80 mg L^{-1}; c_e: equilibrium concentration in the aqueous phase of amararnth; pH 4.0). (B) Adsorption rate (●, black) and adsorption isothermal (●, blue) of amaranth on 150 g L^{-1} of the FeOOH/AC heterogeneous catalysts. Aqueous amaranth solutions with different initial concentrations varied from 10 to 80 mg L^{-1}.

6A). It can be seen that the increase in catalyst loading amount resulted in higher initial color removal rates of amaranth. The adsorption process of amaranth on the three different loading amounts of FeOOH/AC heterogeneous catalysts closely approached equilibrium within 15 min, and no significant changes were observed from 15 to 240 min. The fast dynamic equilibrium process of adsorption indicated that the transformation between the adsorbed state and the dissolved state of amaranth was very easy and quick. About 29.6, 34.8, and 39.7% amaranth was adsorbed on 100, 150, and 200 g L^{-1} FeOOH/AC heterogeneous catalysts, respectively. The saturated adsorption amounts are appreciable, implying the admirable

dx.doi.org/10.1021/jp210167b | J. Phys. Chem. C 2012, 116, 3623−3634

Table 2. Langmuir and Freundlich Adsorption Kinetic Parameters Calculated from Equations 7 and 8 for Amaranth Adsorption on the FeOOH/AC Heterogeneous Catalysts

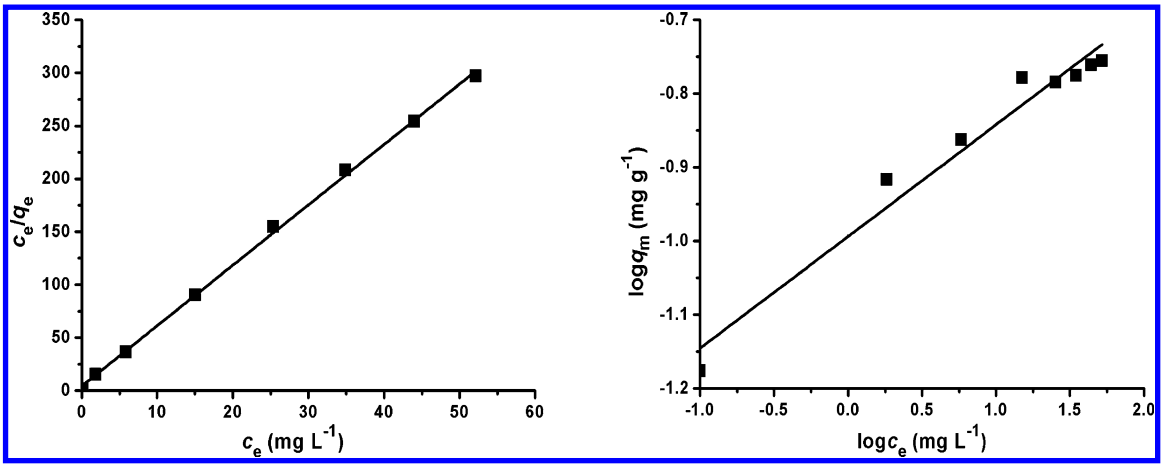

Langmuir				Freundlich		
$1/(K_L q_m)$	$1/q_m$	R^2	R_L	K_F	$1/n$	R^2
5.701	4.378	0.9988	0.016	0.1089	0.1516	0.9596

adsorbability of the FeOOH/AC heterogeneous catalysts. On the basis of characterization results, we can relate this performance to both its mesoporous structure and relatively high surface area. Additionally, it can be also explained according to the isoelectric point, that is, the zero charge point of FeOOH (pH_{zpc} ca. 6.4 to 7.7).[2,5] The FeOOH/AC heterogeneous catalyst carried a positive charge between pH 4.0 and 6.4 to 7.7, and thus the adsorption of negative charged amaranth bonding with sulfonate group on the FeOOH/AC heterogeneous catalyst takes place spontaneously via the electrostatic interaction. The similar result has also been commonly observed in the study of simple organic matter adsorption on iron oxide.[52]

Aqueous amaranth solutions with different initial concentrations varying from 10 to 80 mg L^{-1} were used for the adsorption experiment. Figure 6B shows the adsorption rate and the adsorption isothermal of amaranth on 150 g L^{-1} FeOOH/AC heterogeneous catalysts. It is found that the adsorption rate decreases gradually, and the adsorption amount increases obviously with the increase in original amaranth concentration, whereas no significant change in the adsorption amount was observed for original amaranth concentration larger than 40 mg L^{-1}, indicating the adsorption equilibrium. As seen in Table 2, the adsorption isotherm of amaranth in the concentration range studied was described using Langmuir and Freundich models represented by eqs 7 and 8, respectively.

Langmuir:

$$\frac{c_e}{q_e} = \frac{1}{K_L q_m} + \frac{c_e}{q_m} \tag{7}$$

Freundlich:

$$\log q_m = \log K_F + \frac{\log c_e}{n} \tag{8}$$

where q_e (mg g^{-1}) is the adsorbed amount of amaranth per unit weight of adsorbent, c_e (mg L^{-1}) is the equilibrium concentration in the solution, q_m (mg g^{-1}) is the maximum adsorption capacity, K_L (L mg^{-1}) is the constant related to the free energy of adsorption, K_F is adsorption coefficient, and $1/n$ represents the nonlinear degree of adsorption. In comparison, it is clear that the Langmuir model is more appropriate and exhibits better linear correlation than the Freundich model, implying that the adsorption of amaranth on the FeOOH/AC heterogeneous catalysts was monolayer adsorption. Additionally, it must also be pointed out that for the Langmuir-type adsorption process the influence of the isotherm shape on whether adsorption is favorable or unfavorable can be classified by the separation factor R_L (eq 9), which is considered as a more reliable indicator of the adsorption capacity.[53]

$$R_L = \frac{1}{1 + K_L c_0} \tag{9}$$

Favorable adsorption is reported when the R_L values are between 0 and 1. In the present work, the value of R_L calculated is 0.016 (Table 2), indicating that the Langmuir model can describe the adsorption process.

3.5. Adsorption and Electrochemical-Assisted Oxidation Performance. Carbon materials such as graphite and AC used as heterogeneous catalysts were reported to have catalytic ability in heterogeneous Fenton reactions because they can activate H_2O_2 and produce free radicals such as superoxide ion.[54,55] However, the contribution of the direct catalysis via the bare carbon materials to the improved degradation performance of target organics was generally very limited. Moreover, most authors considered that the synergistic effect derived from the adsorption property of support caused the difference in substrate degradation rate. It is reported that the adsorbed substrate on support was nearly unreactive, and adsorption on AC surface had an adverse effect on the oxidation of organic contaminants via $HO^{\bullet}$ radicals. On the contrary, the organic pollutant molecules dissolved freely in the aqueous pore volume of AC can be readily attacked by $HO^{\bullet}$ species resulting in the predominant degradation of organics.[56] The above-reported results were favorable to make the authors think that the adsorbed amaranth molecules in the immediate vicinity of immobilized Fe ions were easily attacked by $HO^{\bullet}$ radicals; in other words, amaranth adsorption on the FeOOH/AC heterogeneous catalysts should possess the positive effect on its degradation.

dx.doi.org/10.1021/jp210167b | J. Phys. Chem. C 2012, 116, 3623−3634

Before electrolysis, the overall system was maintained in open circuit status for 30 min to ensure the adsorption equilibrium of amaranth on the FeOOH/AC heterogeneous catalysts. Then, power on and commence the electrochemically assisted oxidation process. The initial soluble iron concentration is listed in Table 3. Cassano et al.[2] have proposed three

Table 3. Initial and Final Soluble Iron Concentrations during the Treatment Using the FeOOH/AC Heterogeneous Catalyst with Different Loading Amounts

	initial soluble iron concentration (mg L^{-1})[a]			final soluble iron concentration (mg L^{-1})		
catalyst loading amount (g L^{-1})	Fe^{2+}	Fe^{3+}	Fe_{Total}	Fe^{2+}	Fe^{3+}	Fe_{Total}
100		12.42	12.42	1.63	2.63	4.26
150		13.89	13.89	1.68	3.81	5.49
200		16.72	16.72	1.98	6.65	8.63

[a]Soluble iron concentration when amaranth achieving the adsorption equilibrium on the FeOOH/AC heterogeneous catalysts.

typical heterogeneous surface reactions including proton promoted iron dissolution reaction, electron-donor-involved reduction reaction, and nonreductive ligand dissolution reaction, through which iron can be released into the bulk solution. In our work, there is no external electric field or electron donor in amaranth adsorption equilibrium period, and thus a single-proton-promoted dissolution step (eqs 10 and 11), which produces Fe^{3+}, is dominate in this stage. Similar behavior has also been investigated in details by Lu et al.[27,29] with the same conclusions.

$$FeOOH_{solid} + 3H^+ \rightarrow Fe_{ads}^{3+} + 2H_2O \quad (10)$$

$$Fe_{ads}^{3+} \Leftrightarrow Fe_{aq}^{3+} \quad (11)$$

This is feasible because in pH 4.0 solution the surface of nano-FeOOH will be surrounded by a high concentration of protons. It is known that goethite (hexagonal packing structure) and lepidocrocite (cubic packing structure) are not the dense iron oxides, and both have empty octahedral sites, which render nano-FeOOH lattice more accessible to the diffusion of small H^+ into its inner structure. It is reported that on the FeOOH surface the first step of proton-induced dissolution of iron involves the formation of $O{=}Fe^{III}(OH_2)_2^+$ which weakens the $Fe^{III}{-}O$ bond and thus promotes the detachment of Fe^{III} to the solid/solution interface.[2] This Fe^{3+} liberation from nano-FeOOH structure to the solution (eq 10) has been reported to be slower than the subsequent reaction due to the diffusion mass transfer limitations of Fe^{3+} inside the pores of catalyst or at the external boundary layer of the solid/solution interface.

As seen from Figure 7A, some sort of delay in dye color abatement was observed for the three different catalyst loadings in the first 60 min after power on. This is mostly related to: (i) The covering of FeOOH/AC active sites with adsorbed amaranth delays the start of catalyst activity owing to the oxidation of adsorbed amaranth by the electrogenerated reactive oxygen species. (ii) Although the electrochemical reciprocal transformation of Fe^{3+}/Fe^{2+} redox couple is fast, whereas the required iron concentration to generate sufficient $HO^\bullet$ radicals for effective amaranth decolorization is not an instantaneous realization process due to the slow mass transfer

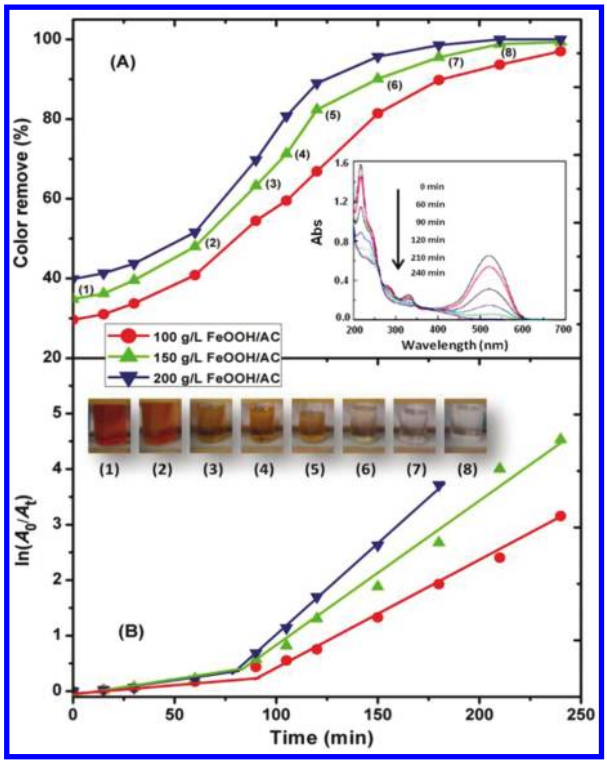

Figure 7. (A) Electrochemically assisted oxidative decolorization of amaranth on the FeOOH/AC heterogeneous catalyst with different loading amounts. Adsorption equilibrium of amaranth on the FeOOH/AC heterogeneous catalysts was achieved by maintaining open circuit status for 30 min. (B) Corresponding kinetics analysis assuming a combined two-stage pseudo-first-order reaction in the case of adding 150 g L^{-1} FeOOH/AC heterogeneous catalyst as iron resource. The inset presents the changes of UV−vis spectrum and dye color. Applied cathodic potential: −0.64 V, the electrolyte: 80 mg L^{-1} amaranth + 0.2 mol L^{-1} Na_2SO_4, solution pH: 4.0.

of Fe^{3+} from the solid/solution interface into the bulk solution. (iii) The preponderant generation of weaker oxidant $HO_2^\bullet$ (eqs 12 and 13) due to the initial proton promoted dissolution of Fe^{3+} from nano-FeOOH surface in amaranth adsorption equilibrium period.

$$Fe_{aq}^{3+} + H_2O_2 \rightarrow Fe_{aq}^{2+} + HO_2^\bullet + H^+ \quad (12)$$

$$Fe_{ads}^{3+} + H_2O_2 \rightarrow Fe_{ads}^{2+} + HO_2^\bullet + H^+ \quad (13)$$

After 60 min electrolysis, the exposed FeOOH/AC active sites increase accordingly with the decrease in adsorbed amaranth. Meanwhile, the graphite felt cathode donates electrons to enhance Fe^{2+} dissolution from nano-FeOOH (eq 14), which can increase the reaction rate of homogeneous Fenton process (eq 15) and produce an appreciable amount of $HO^\bullet$ radicals.

$$FeOOH_{solid} + 3H^+ + e^- \rightarrow Fe_{aq}^{2+} + 2H_2O \quad (14)$$

$$Fe_{aq}^{2+} + H_2O_2 \rightarrow Fe_{aq}^{3+} + HO^\bullet + OH^- \quad (15)$$

Additionally, the heterogeneous Fenton reactions between the electrogenerated H_2O_2 and Fe_{ads}^{3+} (eq 13) or Fe_{ads}^{3+} (eqs 16 and 17) could generate a certain amount of efficacious $HO_2^\bullet$ and $HO^\bullet$ radicals that would contribute to dye degradation and decolorization rates. In this case, the adsorption of FeOOH/AC

dx.doi.org/10.1021/jp210167b | J. Phys. Chem. C 2012, 116, 3623−3634

near the catalytic active center of nano-FeOOH was favorable to the enhancement of the decolorization efficiency of residual dye in aqueous solution.

$$Fe_{ads}^{3+} + e^- \rightarrow Fe_{ads}^{2+} \quad (16)$$

$$Fe_{ads}^{2+} + H_2O_2 \rightarrow Fe_{ads}^{3+} + HO^{\bullet} + OH^- \quad (17)$$

The beneficial effect of combined homogeneous/heterogeneous electro-Fenton oxidation was relatively obvious. As seen from the inset in Figure.7A, significant dye decays were observed in all cases, as revealed by the color and UV−vis spectrum changes, taking the 150 g L^{-1} FeOOH/AC heterogeneous catalyst loading, for example. After ca. 240 min electrolysis, the whole conjugated chromophore structures of amaranth were completely cleaved because the characteristic absorption band around 521 nm totally disappeared. Although the reductive dissolution of nano-FeOOH is always on during the experiment, only small quantities of dissolved iron were obtained (Table 3) at the end of treatment due to the precipitation or readsorption of ferric ions on the nano-FeOOH surface. The above results indicate that the electrochemically assisted oxidative degradation/decolorization process of amaranth by $HO^{\bullet}$ radicals occurs not only on the catalyst surface (heterogeneous Fenton reaction) but also in the aqueous solution (homogeneous Fenton reaction) through iron dissolution of the supported nano-FeOOH.

To analyze the kinetics of amaranth decolorization process, we present the plots of $\ln(A_0/A_t)$ versus time in Figure 7B. It can be seen that the two-stage pseudo-first-order reaction kinetics can describe satisfactorily for dye color decay for all catalyst loadings. This so-called combined pseudo-first-order kinetics can be represented by eq 18.[57]

$$A = A_{01}\exp(-k_{app1}t) + A_{02}\exp(-k_{app2}t) \quad (18)$$

where A_{01} and A_{02} are the initial dye absorbances and k_{app1} and k_{app2} are the apparent rate constants of the two independent pseudo-first-order reactions, respectively. The apparent rate constants of each stage were obtained from the slopes of straight lines of Figure 7B and are reported in Table 4. As seen, the first stages have lower rate constants because of the covering of nano-FeOOH reactive sites and the oxidation of adsorbed amaranth mainly by $HO_2^{\bullet}$ radicals. The much higher reaction rate constants in the second stage should be attributed to the exposure of nano-FeOOH reactive sites and the electrochmical reductive dissolution of Fe^{2+} from the supported nano-FeOOH.

Table 4. Apparent Rate Constants for the Two-Stage Pseudo-First-Order Kinetics in the Oxidative Decolorization Process of Amaranth Using the FeOOH/AC Heterogeneous Catalyst with Different Loading Amounts

	first-stage		second-stage	
catalyst loading amount (g L^{-1})	k_{app1} ($\times 10^3$ min^{-1})	R^2	k_{app2} ($\times 10^2$ min^{-1})	R^2
100	2.97	0.9477	1.83	0.9901
150	3.71	0.9386	2.74	0.9840
200	3.89	0.9289	3.36	0.9988

3.6. Contribution Proportions of Homogeneous Catalysis and Heterogeneous Catalysis. As discussed above, the nano-FeOOH-catalyzed electrochemical oxidation of amaranth is promoted by the homogeneous catalysis through the reductive dissolution of iron ions from nano-FeOOH and by the heterogeneous catalysis at nano-FeOOH surface. To quantify the contribution proportions of homogeneous and heterogeneous Fenton reactions, we conducted a parallel oxidation process with an equivalent concentration of soluble ferrous ion. The experiments were carried out by adding 13.9 mg L^{-1} iron (as $FeSO_4$) as the sole iron source in the presence (trial I) and absence (trial II) of 150 g L^{-1} FeOOH/AC solid catalyst. Similarly, the adsorption equilibrium of amaranth on the FeOOH/AC heterogeneous catalysts was also conducted by maintaining open circuit for 30 min before electrolysis. Other experimental conditions are the same as those conducted in Figure 7A.

Soluble ferrous catalyzed homogeneous Fenton oxidation (trial I) in relation to the nano-FeOOH solid catalyzed heterogeneous oxidation (trial II, which consists of both homogeneous and heterogeneous Fenton processes) is shown in Figure 8, from which the degree of heterogeneous and homogeneous catalysis can be estimated roughly. As can be observed, the homogeneous Fenton oxidation process achieved 16.1% of dye decolorization rate, whereas a 3.82% of color remove was obtained through the heterogeneous-catalyzed process during the first 60 min. Therefore, the homogeneous Fenton oxidation was ~80.8% over the first 60 min. After 60 min, the contribution of heterogeneous-catalyzed oxidation increased gradually, whereas a similar "platform-like behavior" as that reported in literature[18,21,49] was obtained in the homogeneous Fenton oxidation process, implying that Fe^{2+} regeneration (eq 12) and $HO^{\bullet}$ radicals formation (eq 3) in the solution are anyhow restricted by the lower concentration of soluble Fe^{2+} compared with the optimal Fe^{2+} concentration (1.0 mM)[16,18,21] of the homogeneous electro-Fenton process. At 180 min, the homogeneous and heterogeneous Fenton oxidation process achieved 31.78 and 29.32% of dye decolorization rates; therefore, the oxidation attributed to the heterogeneous catalysis was ca. 47.98%. The above results demonstrate that the heterogeneous catalysis reactions provide a mechanism of amaranth oxidation in addition to the soluble iron-catalyzed oxidations.

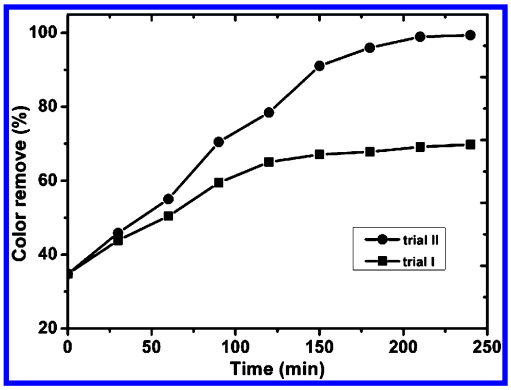

Figure 8. Amaranth color abatement rate during electro-oxidation in the cases of adding 13.9 mg L^{-1} iron (as $FeSO_4$) as the sole iron source in the absence (trial I) and presence (trial II) of 150 g L^{-1} FeOOH/AC heterogeneous catalyst. The experimental conditions of trials I and II are the same as those in Figure 7A.

The complete disappearance of amaranth is not an indication that all of the organic compounds present in the solution have been degraded thoroughly because of the formation of

dx.doi.org/10.1021/jp210167b | J. Phys. Chem. C 2012, 116, 3623−3634

oxidation intermediates. Therefore, the mineralization of amaranth was monitored by measuring TOC of the solution during the electrolysis of 80 mg L^{-1} dye solution under the conditions of adding various loading amounts of FeOOH/AC heterogeneous catalysts. The TOC removal-time profile is presented in Figure 9. The faster decrease in dye color in Figure 7A compared with solution TOC removal indicated the production of some intermediates during the electrochemically assisted oxidation process.

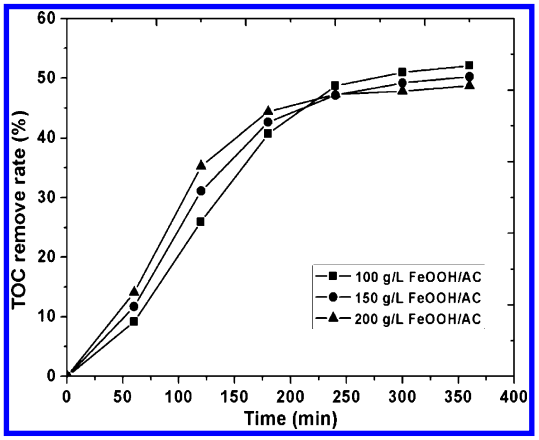

Figure 9. TOC removal rate changes versus time during the electrochemically assisted oxidation of amaranth on the FeOOH/AC heterogeneous catalyst with different loading amounts.

In the present work, H_2O_2 is electrogenerated continuously. This avoids the side reaction that excessive H_2O_2 can bring about $HO^•$ radicals scavenging effect. In general, the large initial input of H_2O_2 in traditional Fenton system needs shorter reaction time for the target pollutants degradation but achieves relatively low organics removal efficiency. From Figure 9, it can be observed that all three cases show rapid mineralization and the TOC removal rate increased with the increase in catalyst loadings during the first 180 min electrolysis, which is in good accordance with the fact that the higher reaction rate of electrocatalytic degradation is expected by increasing the catalyst dose. However, at longer electrolysis times, a distinct decrease in TOC removal rate is observed in all three cases. All heterogeneous catalytic systems tend to reach a maximum value for TOC remove after 6 h of reaction. This upper limit is probably set for the total oxidation of amaranth and the appearance of refractory carboxylic acids, which are not suitable to be completely mineralized under the present reaction conditions.

The comparison of three plots indicates that the use of 200 g L^{-1} FeOOH/AC as heterogeneous iron source produced the lowest final mineralization degree at the end of treatment. (Actually, the achieved mineralization efficiency is very close.) The reason for this behavior is that usually high catalyst loadings lead to the high dissolved Fe^{3+} concentration (see Table 3) in the solution. The dissolved Fe^{3+} can facilitate the Fe^{3+}-oxalate and Fe^{3+}-carboxylic acid complexes formation[1,15] and in turn results in a lower TOC removal rate due to the difficult in total mineralization of these Fe^{3+}-complexes, especially Fe^{3+}-oxalate by $HO^•$ radicals only.[18,21] Chiou et al.[58] suggested from the homogeneous catalytic reaction of H_2O_2 and Fe^{2+} that leaching from iron oxides is dominant and significant, whereas the heterogeneous reaction of H_2O_2 with the iron contained in the solid lattice plays a negligible role in the mineralization of organic compounds, except for the adsorption of organics on iron oxide surface.

Additionally, it is now believed that low solid catalyst concentration and high reaction temperature are important factors for satisfactory organics degradation and reasonable mineralization degree. However, high heterogeneous catalyst loadings and high reaction temperature in any case give rise to the noneffective consumption of H_2O_2 regardless of organics degradation effect.[2,59−61] At low pH media as the one used in the present work, the catalytic action of nano-FeOOH in the heterogeneous Fenton reaction results in the solid catalyzed unproductive decomposition of H_2O_2 through eq 19; in other words, in this heterogeneous Fenton reaction, the consumption rate of H_2O_2 does not equal to the generation rate of $HO^•$ radicals because H_2O_2 can be additionally decomposed to water and oxygen via nonradical producing pathways by nano-FeOOH catalysts. Therefore, the noncontributive decomposition of H_2O_2 interferes with the $HO^•$ radicals production and consequently leads to the decrease in its efficient oxidation toward amaranth.

$$H_2O_2 \xrightarrow{FeOOH_{solid}} H_2O + \frac{1}{2}O_2 \qquad (19)$$

3.7. Approaching the Catalytic Mechanism. Goethite and lepidocrocite used as iron source for electro-Fenton oxidation process has been previously reported. Although goethite and lepidocrocite possess low-soluble FeOOH, these minerals could undergo reductive dissolution via releasing iron ions into the solution.[1,4,13] The primary mechanisms for the adsorption and electrochemically assisted oxidation of amaranth may be depicted as follows according to the above obtained results.

In amaranth adsorption equilibrium period, Fe_{ads}^{3+} would be produced first through the proton-promoted dissolution of iron from nano-FeOOH (eq 10) under the present weak acidic condition. Then, Fe_{ads}^{3+} is released slowly through the solid/solution interface and finally is transferred into the bulk solution, as described in eq 11. After power on, Fe_{aq}^{2+} would be produced through the electrochemical reduction of supported nano-FeOOH according to eq 14. Meanwhile, Fe_{ads}^{3+} and Fe_{aq}^{3+} generated in amaranth adsorption equilibrium period would also be reduced to form Fe_{ads}^{2+} and Fe_{aq}^{2+}, respectively. The reduction process takes place until the catalyst surface becomes saturated by Fe_{ads}^{2+}; then, Fe_{ads}^{2+} is released from the solid/solution interface into the bulk solution achieving equilibrium with Fe_{aq}^{2+} in the vicinity of catalyst surface. In addition, the electrochemical ORR on graphite felt cathode producing H_2O_2 took place simultaneously (eq 3). Finally, the iron ions reacted with H_2O_2 through heterogeneous and homogeneous catalytic pathways to generate $HO^•$ (eqs 15 and 17) and $HO_2^•$ (eqs 12 and 13), leading to amaranth degradation.

4. CONCLUSIONS

The supported nano-FeOOH catalysts prepared by air oxidation of ferrous hydroxide suspension method were characterized by various techniques and were identified as goethite and lepidocrocite mixed crystals coated on activated carbon supports. Under weak acidic and external electric field conditions, the electrogeneration of Fe^{2+} and H_2O_2 from the supported nano-FeOOH catalysts and the dissolved oxygen, respectively, took place concurrently in cathodic region. The FeOOH/AC heterogeneous catalyst has been proven to

possess admirable adsorbability. Amaranth can be efficiently degraded not only through the heterogeneous Fenton reaction on the catalyst/solution interface but also through the homogeneous Fenton reaction in the bulk solution, which is based on the introduction of iron ions into the solution by two different mechanisms: (i) an interfacial proton-promoted dissolution reaction of ferric ions on nano-FeOOH surface under the acidic condition and (ii) surface and liquidus electrochemical reductive liberation of iron species under the external electric field condition, which facilitate the regeneration of ferrous ions and produce a beneficial enhancement of the homogeneous and heterogeneous Fenton reaction rates. These characteristics made it possible to apply the supported nano-FeOOH as heterogeneous catalysts to the practical Fenton oxidation treatment of contaminated waters even for the mineralization purposes.

AUTHOR INFORMATION

Corresponding Author

*E-mail: guoquanz@126.com.

ACKNOWLEDGMENTS

We acknowledge the financial support from the National Natural Science Foundation of China (grant no. 21177017), the Fundamental Research Funds for the Central Universities, and the Post-Doctoral Science Foundation of China (grant no. 20080440169).

REFERENCES

(1) Sánchez-Sánchez, C. M.; Expósito, E.; Casado, J.; Montiel, V. *Electrochem. Commun.* **2007**, *9*, 19−24.

(2) Ortiz de la Plata, G. B.; Alfano, O. M.; Cassano, A. E. *Appl. Catal. B: Environ.* **2010**, *95*, 1−13.

(3) Ortiz de la Plata, G. B.; Alfano, O. M.; Cassano, A. E. *Appl. Catal. B: Environ.* **2010**, *95*, 14−25.

(4) Du, W. P.; Xu, Y. M.; Wang, Y. S. *Langmuir* **2008**, *24*, 175−181.

(5) Chou, S. S.; Huang, C. P.; Huang, Y. H. *Environ. Sci. Technol.* **2001**, *35*, 1247−1251.

(6) Chou, S. S.; Huang, C. P. *Chemosphere* **1999**, *38*, 2719−2731.

(7) Liang, X. L.; Zhong, Y. H.; Zhu, S. Y.; Zhu, J. X.; Yuan, P.; He, H. P.; Zhang, J. *J. Hazard. Mater.* **2010**, *181*, 112−120.

(8) Wang, Y.; Du, W. P.; Xu, Y. M. *Langmuir* **2009**, *25*, 2895−2899.

(9) Li, Y.; Lu, A. H.; Ding, H. R.; Wang, X.; Wang, C. Q.; Zeng, C. P.; Yan, Y. H. *Electrochem. Commun.* **2010**, *12*, 944−947.

(10) Barreiro, J. C.; Capelato, M. D.; Martin-Neto, L.; Hansen, H. C. B. *Water Res.* **2007**, *41*, 55−62.

(11) Ai, Z. H.; Lu, L. R.; Li, J. P.; Zhang, L. Z.; Qiu, J. R.; Wu, M. H. *J. Phys. Chem. C* **2007**, *111*, 4087−4093.

(12) Deng, J. H.; Jiang, J. Y.; Zhang, Y. Y.; Lin, X. P.; Du, C. M.; Xiong, Y. *Appl. Catal. B: Environ.* **2008**, *84*, 468−473.

(13) Mazille, F.; Schoettl, T.; Klamerth, N.; Malato, S.; Pulgarin, C. *Water Res.* **2010**, *44*, 3029−3038.

(14) Feng, H. M.; Zheng, J. C.; Lei, N. Y.; Yu, L.; Kong, K. H.-K.; Yu, H. Q.; Lau, T. C.; Lam, M.H. W. *Environ. Sci. Technol.* **2011**, *45*, 744−750.

(15) Huang, R. H.; Yan, H. H.; Li, L. S.; Deng, D. Y.; Shu, Y. H.; Zhang, Q. Y. *Appl. Catal. B: Environ.* **2011**, *10*, 6264−271.

(16) Expósito, E.; Sánchez-Sánchez, C. M.; Montielz, V. *J. Electrochem. Soc.* **2007**, *154*, E116−E122.

(17) Nie, Y. L.; Hu, C.; Zhou, L.; Qu, J. H. *Appl. Catal. B: Environ.* **2008**, *82*, 151−156.

(18) Brillas, E.; Sirés, I.; Oturan, M. A. *Chem. Rev.* **2009**, *109*, 6570−6631.

(19) Zhang, G. Q.; Wang, S.; Zhao, S.; Fu, L.; Chen, G. H.; Yang, F. L. *Appl. Catal. B: Environ.* **2011**, *106*, 370−378.

(20) Ruiz, E. J.; Arias, C.; Brillas, E.; Hernández-Ramírez, A.; Peralta-Hernández, J. M. *Chemosphere* **2011**, *82*, 495−501.

(21) Martínez-Huitle, C. A.; Brillas, E. *Appl. Catal. B: Environ.* **2009**, *87*, 105−145.

(22) Zhang, G. Q.; Yang, F. L.; Liu, L. F. *J. Electroanal. Chem.* **2009**, *632*, 154−161.

(23) Matta, R.; Hanna, K.; Chiron, S. *Sci. Total Environ.* **2007**, *385*, 242−251.

(24) Khan, MD. A. J.; Watts, R. J. *Water, Air, Soil Pollut.* **1996**, *88*, 247−260.

(25) Chiou, C. S.; Chang, C. F.; Chang, C. T.; Shie, J. L.; Chen, Y. H. *Chemosphere* **2006**, *62*, 788−795.

(26) Teel, A. L.; Warberg, C. R.; Atkinson, D. A.; Watts, R. J. *Water Res.* **2001**, *35*, 977−984.

(27) Lu, M. C. *Chemosphere* **2000**, *40*, 125−130.

(28) Lin, Y. T.; Lu, M. C. *Water Sci. Technol.* **2007**, *55*, 101−106.

(29) Lu, M. C.; Chen, J. N.; Huang, H. H. *Chemosphere* **2002**, *46*, 131−136.

(30) Bandara, J.; Klehm, U.; Kiwi, J. *Appl. Catal. B: Environ.* **2007**, *76*, 73−81.

(31) Cheng, M.; Song, W.; Ma, W.; Chen, C.; Zhao, J.; Lin, J.; Zhu, H. *Appl. Catal. B: Environ.* **2008**, *77*, 355−363.

(32) Pignatello, J. J.; Oliveros, E.; MacKay, A. *Environ. Sci. Technol.* **2006**, *36*, 1−84.

(33) Liu, H.; Wang, C.; Li, X. Z.; Xuan, X. L.; Jiang, C. C.; Cui, H. N. *Environ. Sci. Technol.* **2007**, *41*, 2937−2942.

(34) Yu, J. G.; Zhang, L. J.; Cheng, B.; Su, Y. R. *J. Phys. Chem. C* **2007**, *111*, 10582−10589.

(35) Kruk, M.; Jaroniec, M. *Chem. Mater.* **2001**, *13*, 3169−3183.

(36) Sing, K. S. W.; Everett, D. H.; Haul, R. A. W.; Moscou, L.; Pierotti, R. A.; Rouquerol, J.; Siemieniewska, T. *Pure Appl. Chem.* **1985**, *57*, 603−619.

(37) Christensena, A. N.; Jensenb, T. R.; Bahlc, C. R. H.; DiMasi, E. *J. Solid State Chem.* **2007**, *180*, 1431−1435.

(38) Ishikawa, T.; Takeuchi, K.; Kandori, K.; Nakayama, T. *Colloids Surf., A* **2005**, *266*, 155−159.

(39) Lin, R. G.; Spicer, R. L.; Tungate, F. L.; Davis, B. H. *Colloids Surf., A* **1996**, *113*, 79−96.

(40) Srinivasan, R.; Lin, R. G.; Spicer, R. L.; Davis, B. H. *Colloids Surf. A* **1996**, *113*, 97−105.

(41) Cornell, R. M.; Schwertmann, U. *The Iron Oxides*; VCH Publishers: New York, 1996.

(42) Ristić, M.; Musić, S.; Godec, M. *J. Alloys Compd.* **2006**, *417*, 292−299.

(43) Weckler, B.; Lutz, H. D. *Eur. J. Solid State Inorg. Chem.* **1998**, *35*, 531−544.

(44) Chen, R. F.; Chen, H. X.; Wei, Y.; Hou, D. L. *J. Phys. Chem. C* **2007**, *111*, 16453−16459.

(45) Panizza, M.; Cerisola, G. *Water Res.* **2001**, *35*, 3987−3992.

(46) Panizza, M.; Oturan, M. A. *Electrochim. Acta* **2011**, *56*, 7084−7087.

(47) Ozcan, A.; Oturan, M. A.; Oturan, N.; Sahin, Y. *J. Hazard. Mater.* **2009**, *163*, 1213−1220.

(48) Zhang, G. Q.; Yang, F. L. *Electrochim. Acta* **2007**, *52*, 6595−6603.

(49) Zhang, G. Q.; Yang, F. L.; Gao, M. M.; Liu, L. F. *J. Phys. Chem. C* **2008**, *112*, 8957−8962.

(50) Vaik, K.; Schiffrin, D. J.; Tammeveski, K. *Electrochem. Commun.* **2004**, *6*, 1−5.

(51) Ma, J. H.; Ma, W. H.; Song, W. J; Chen, C. C.; Tang, Y. L.; Zhao, J. C.; Huang, Y. P.; Xu, Y. M.; Zang, L. *Environ. Sci. Technol.* **2006**, *40*, 618−624.

(52) Gu, B.; Schmitt, J.; Chen, Z.; Liang, L.; McCarthy, J. F. *Environ. Sci. Technol.* **1994**, *25*, 38−46.

(53) Mouzdahir, Y.; El ; Elmchaouri, A.; Mahboub, R.; Gil, A.; Korili, S. A. *J. Chem. Eng. Data* **2007**, *52*, 1621−1625.

(54) Maldonado-Hodar, F. J.; Madeira, L. M.; Portela, M. F. *Appl. Catal. A: Gen.* **1999**, *178*, 49−60.

(55) Lücking, F.; Köer, H.; Jank, M.; Ritter, A. *Water Res.* **1998**, *32*, 2607−2614.
(56) Georgi, A.; Kopinke, F. D. *Appl. Catal. B: Environ.* **2005**, *58*, 9−18.
(57) Guivarch, E.; Trevin, S.; Lahitt, C.; Oturan., M. A. *Environ. Chem. Lett.* **2003**, *1*, 38−44.
(58) Chiou, C. S.; Chang, C. F.; Chang, C. T.; Shie, J. L.; Chen, Y. H. *Chemosphere* **2006**, *62*, 788−795.
(59) Pignatello, J. J.; Oliveros, E.; MacKay, A. *Crit. Rev. Environ. Sci. Technol.* **2006**, *36*, 1−84.
(60) Teel, A. L.; Finn, D. D.; Schmidt, J. T.; Cutler, L. M.; Watts, R. J. *J. Environ. Eng.* **2007**, *133*, 853−858.
(61) Lin, S.-S. *Interaction of H_2O_2 with Iron Oxide for Oxidation of Organic Compounds in Water*, Ph.D. Thesis, Drexel University, 1997.